UC Berkeley
UC Berkeley Previously Published Works

Title
On seismic response of stiff and flexible retaining structures

Permalink
https://escholarship.org/uc/item/8gb0j4mz

Authors
Wagner, Nathaniel
Sitar, Nicholas

Publication Date
2016-12-01

DOI
10.1016/j.soildyn.2016.09.025

Peer reviewed

eScholarship.org Powered by the California Digital Library
University of California

On seismic response of stiff and flexible retaining structures

Nathaniel Wagner[a], Nicholas Sitar[b,*]

[a] SAGE Engineers, Oakland, CA, USA [b] Civil and Environmental Engineering, University of California Berkeley, 449 Davis Hall, Berkeley, CA 94720, USA

* Corresponding author. E-mail addresses: nbwagner@sageengineers.com (N. Wagner), sitar@berkeley.edu (N. Sitar).

Abstract

This paper presents an overview of the results of experimental and analytical studies of the seismic response of stiff and flexible retaining structures. These studies were motivated by very large dynamic forces in areas of high seismicity predicted by current seismic design methodologies based on the work of Okabe [3] and Mononobe and Matsuo [4]. However, there is no evidence of systematic failures of retaining structures in major earthquakes even when the ground accelerations clearly exceeded the design assumptions. The experimental program consisted of a series of geotechnical centrifuge model studies with different types of structures with cohesionless and cohesive backfill. Overall, the results of these studies show that the Mononobe-Okabe (M-O) method of analysis provides a reasonable upper bound for the response of stiff retaining structures and that flexible retaining structures experience loads significantly smaller than those predicted by this method. Moreover, for deep embedded structures the dynamic forces do not continue to increase with depth and gradually become a small fraction of the overall load on the walls.

Keywords: Seismic earth pressure, Retaining structure, Basement, Centrifuge modeling, Numerical modeling

1. Introduction

The introduction of more stringent seismic design provisions in recent updates of design codes, e.g. IBC 2012 [1] and FEMA 750 [2], has increased the demand on seismic design of retaining walls and basement structures and, hence, there is a need for an appropriate analysis and design methodology. While not all codes are prescriptive in specifying a particular methodology, the most commonly recommended analyses for cantilever and gravity structures are based on a limit equilibrium method developed in the 1920's in Japan by Okabe [3] and Mononobe and Matsuo [4], generally referred to as the Mononobe-Okabe method. While various modifications of this method have been introduced since, e.g. Seed and Whitman [5] and Mylonakis et al. [6], the principal problem for a designer is that at high accelerations, > 0.5*g*, these methods predict very large dynamic forces, which appear unrealistic in view of actual experience in recent earthquakes. The problem of predicting high seismic loads becomes even more pronounced in the design of “non-yielding walls”, defined as structures based on rock or very stiff soil that will not deflect more than 0.002H [2],

which is based on a solution by Wood [7]. An additional complication is that the recommended design procedures make very little difference between different types of retaining structures. Fig. 1 is a schematic representation of some of the typical settings and configurations of retaining structures. Clearly, free-standing cantilever structures that can translate and rotate will respond differently than cantilever sides of channel structures that can flex, but cannot translate, and structures on sloping ground present yet another, completely different scenario. Moreover, structures retaining native ground will experience different loading than structures retaining cohesionless or cohesive backfill.

Sitar et al. [8] present a detailed review of the different methods of analysis and their underlying assumptions and, therefore, the focus of this paper is first on pointing out the fundamental differences in the various approaches that lead to the reported results. Recent experimental results in addition to observations from recent earthquakes are presented to show that the above mentioned traditional analysis methods do not adequately represent the actual seismic demand and that they are indeed conservative.

2. Observed response in recent earthquakes

Before considering the theoretical aspects of the methods of analysis, it is worthwhile to consider the observed performance of retaining structures in recent major earthquakes. A review of the performance of basement walls by Lew et al. [9], drawing on experience from the 1989 Loma Prieta, 1994 Northridge and 1995 Kobe earthquakes, concluded that seismically induced failures of basement walls or deep excavations were rare. In this context it is important to note that many of the older structures were either not at all designed for seismic loading, or even if they were the designed for seismic loading, the design ground motions were significantly smaller than those actually experienced by the structures. When failures did occur they were typically either liquefaction-triggered failures of waterfront structures retaining saturated backfill, or structures on slopes and retaining sloping backfill [8]. Most recently, very few cases of damage of retaining structures occurred in the 2008 Wenchuan earthquake in China, the 2010–2011 Canterbury earthquakes in Christchurch, New Zealand (Kendal Riches, [10]), and in the great subduction earthquakes in Chile in 2010 (Verdugo et al., [11]) and Japan in 2011 [8]. Fig. 2 shows a conventional retaining wall supporting a cut slope adjacent to a fault trace in Sichuan 2008. Except for the offset along the fault (Fig. 2a), there were no other signs of distress. On the other hand, structures with design flaws have experienced distress. Fig. 3 shows a cantilever wall, which rotated about its base in the 2014 Iquique earthquake in Chile. The wall does not have a footing and has essentially no embedment. However, it is not clear if the rotation was caused by the inertia of the wall itself or due to the pressure of the backfill. An adjacent similar height wall showed no distress. Overall, there is no evidence of a systemic problem with well executed, conventional, static or minimal seismic retaining wall design even under quite severe loading conditions. For example Clough

and Fragaszy [12] found that reinforced concrete cantilever structures, well designed and detailed for static loading, performed without any sign of distress at accelerations up to about 0.4*g*. A similar conclusion was reached by Seed and Whitman [5], who suggested that conventionally designed gravity structures should perform satisfactorily under seismic loading up to 0.3*g*.

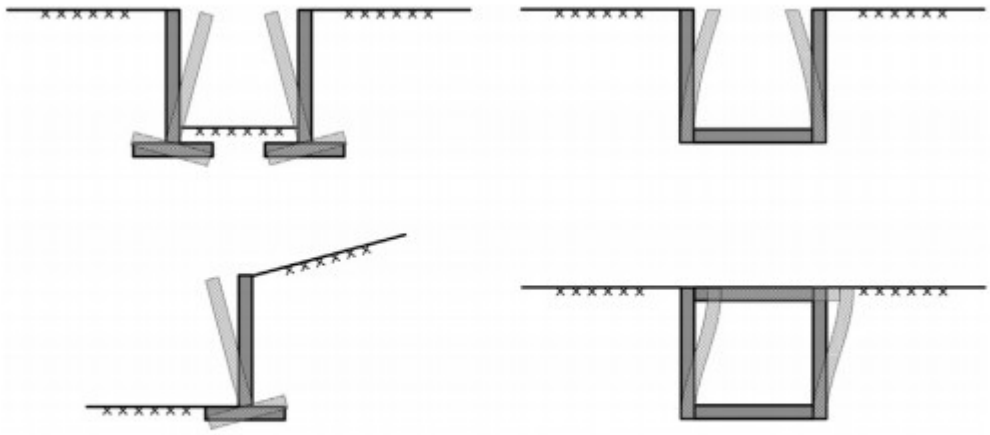

Fig. 1. Schematic illustration of typical retaining structure configurations and deformation modes.

3. Methods of analysis and design

3.1. Conventional gravity and cantilever walls (“Yielding Walls”)

3.1.1. Cohesionless backfill

Conventional gravity and cantilever walls, i.e. walls that can deflect, rotate, and translate, are most commonly designed using the Mononobe-Okabe (M-O) method or, particularly in the US, using the Seed and Whitman [5] simplified approach. Thus, it is of interest to review both methods and to point out the most significant differences. Implicit in both methods is the development of a Coulomb wedge, as shown for the M-O method in Fig. 4a. Hence, an inherent assumption is that the retained soil mass behaves as a rigid body and there is no phase difference between the response of the structure and the soil. Most importantly, the combined static and dynamic force acts at 1/3 H for the M-O method and the active thrust is given by Eq. (1):

$$P_{AE}=0.\ 5\gamma H^2(1-k_v)K_{AE} \qquad (1)$$

where

$$K_{AE}=\frac{\cos^2(\phi-\theta-\beta)}{\cos\theta\cos^2\beta\cos(\delta+\beta+\theta)\left[1+\sqrt{\frac{\sin(\phi+\delta)\sin(\phi-\theta-i)}{\cos(\delta+\beta+\theta)\cos(i-\beta)}}\right]^2} \quad (2)$$

where γ=unit weight of the soil, H=height of the wall, ϕ=angle of internal friction of the soil, δ=angle of wall friction, β=slope of the wall relative to the vertical, i=slope of the backfill relative to the horizontal, $\theta=\tan^{-1}(k_h/(1-k_v))$, k_h=horizontal acceleration (in g), and k_v=vertical acceleration (in g). The horizontal acceleration k_h is often set equal to some fraction of the free field acceleration.

Fig. 2. Conventional retaining structures in the epicentral region of the Wenchuan 2008 Earthquake. Note the fault break in the picture on the right. (Photo: N. Sitar).

Fig. 3. Reinforced concrete wall without a footing rotated during the 2014 Iquique, Chile, earthquake. (Photo courtesy of G. Candia).

A major limitation of Eq. (2) is that it increases exponentially and does not converge if $\theta < \phi - \beta$ (e.g. Kramer [13]), which for typical values of angle of internal friction means accelerations in excess of 0.7g. The alternative introduced by Seed and Whitman [5] is to separate the total force on the wall into its static (P_A) and dynamic (ΔP_{ae}) components. The simplified expression of the dynamic active thrust is given by Eq. (3):

$$\Delta P_{AE} = \frac{1}{2}\gamma H^2 \Delta K_{AE} \Delta K_{AE} \approx \frac{3}{4} k_h \qquad (3)$$

where k_h is the horizontal ground acceleration as a fraction of the acceleration of gravity. Seed and Whitman [5] suggest that k_h be 80% of the

PGA to account for the peak horizontal acceleration only occurring at one instant. This approximation is asymptotically tangent to the M-O solution at accelerations below about 0.4*g* and it remains linear throughout. The most significant difference, however, is in the point of application of the resultant of the dynamic force increment, which Seed and Whitman [5] place at 0.6 H (Fig. 4b). This has led to the concept of an “inverted triangle” to represent the distribution of the dynamic soil pressure on the retaining structure.

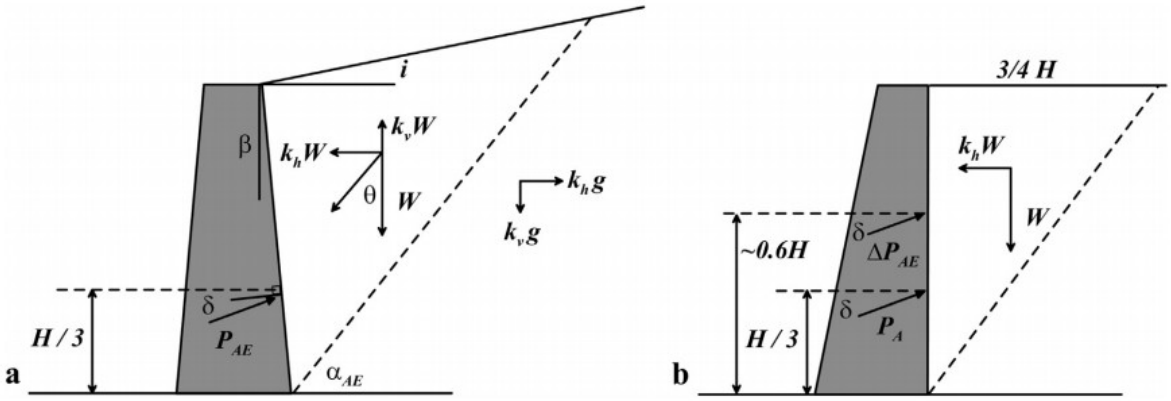

Fig. 4. Force equilibrium diagrams for: a) M-O method (Okabe [3]) and b) Seed and Whitman [5].

The most significant consequence of moving the point of application of the dynamic force increment to 0.6 H is that it essentially doubles the dynamic moment on the structure. While many researchers have weighed in on the issue over the years, it is of note to revisit observations by Mononobe and Matsuo [14]. Specifically, based on their shaking table experiments with sandy backfill, they note that for a very stiff wall the point of application of the dynamic pressure is 0.622 H. However, they also state that for more elastic structure response the point of application should be “h_c/H=1/3 or *less*” and that is what they use in their analyses. In general, experiments on stiff walls with cohesionless backfill on a rigid base on 1-g shaking tables show the same effect, i.e. the maximum dynamic earth pressure increment occurs at 0.4–0.6 H (see e.g. Sherif et al. [15]). In addition to noting that the flexibility of the structure affects the observed dynamic stress increments, Mononobe and Matsuo [14] also observed that a higher degree of compaction also decreased the dynamic soil pressure.

3.1.2. Cohesive backfill

It is important to note that the original M-O method and its derivatives were developed considering purely cohesionless backfill. However, in many typical situations backfill typically has some amount of cohesion and, therefore, it is important to consider it formally in the analyses. Eq. (4) is the full version of Okabe [3] general equation (simplified in Eq. (2)) that includes a cohesion term as follows:

$$K_{AE}=\frac{\sin(\alpha-\phi+\theta)\cos(\alpha-\beta)\left[\cos(\beta-i)+\frac{2q}{\gamma H(1-k_v)}\cos\beta\right]}{\cos^2\beta\cos\theta\sin(\alpha-i)\cos(\alpha-\beta-\phi-\delta)}-\frac{2c}{\gamma H(1-k_v)}\frac{\cos(\beta-i)\cos\phi}{\cos\beta\sin(\alpha-i)\cos(\alpha-\beta-\phi-\delta)} \quad (4)$$

where c=cohesion intercept of the soil and q=uniform surcharge load. This solution suffers from some of the same limitations as Eq. (2) in that it becomes indefinite when $k_h > \tan\phi + 2\,c/\gamma H$. More recently, methods developed by Chen and Liu [16] and Richard and Shi [17], for example, do not suffer from the same limitations. The influence of cohesion (characterized by $\tilde{c}=c/\gamma H$) on the computed seismic earth pressure coefficient is quite significant and should not be neglected, as illustrated in Fig. 5. Specifically, Anderson et al. [18] conclude that the "*reduction for typical design situations could be on the order of about 50 percent to 75 percent*". The good observed seismic performance of retaining structures may in be in part due to the presence of cohesion in typical backfills and in native ground.

3.2. "Non-yielding", stiff retaining structures

As already mentioned, Mononobe and Matsuo [14] observed that stiffer structures, rigidly attached at the base experience higher seismic loads by granular backfill. This problem was first addressed analytically by Wood [7] who modeled linearly elastic soil in a container with rigid walls and a rigid base as shown in Fig. 6a. As can be seen, the computed dynamic stress increment is zero at the base and maximum at the top of the backfill with the recommended point of application of the resulting force at 0.6 H (Fig. 6b). This approach has been adopted by other researchers and similarly high seismically induced earth pressures were computed, e.g. Matsuo and Ohara [19], Prakash [20], Sherif et al. [15], Ostadan and White [21] and Ostadan [22]. However, very few structures are perfectly rigid and FEMA 750 [2] explicitly points out that this solution applies to non-yielding walls "*founded on rock or very stiff soil*". A non-yielding wall is defined as one with deformations < 0.002 H [2]. This same observation was made earlier by Mononobe and Matsuo [14]. Moreover, the solution is strictly applicable only to cohesionless backfill. Thus, care should be exercised in considering this approach in the design of typical retaining structures as it may lead to extremely conservative results.

3.3. Linear Elastic Analytical Solutions

Linear elastic closed form or iterative solutions have been proposed by a number of investigators including Veletsos and Younan [23], Younan and Veletsos [24], Zeng [25], and Steedman and Zeng [26]. While computationally more demanding, these methods offer an alternative to the

limit equilibrium methods and have the advantage that they can consider elastic wave propagation, including wave attenuation and the influence of the relative stiffness of the soil and the structure. Although, these methods cannot handle material nonlinearity and cannot account for energy dissipation should a gap open between the structure and the retained soil, they provide a rigorous solution that can be tested against experimental results. When considering realistic wall stiffness (characterized by $d_w = GH^3/D_w$, where G is the elastic shear modulus of the backfill, H is the backfill height, and $D_w = E_w t_w^3/12(1-\nu_w^2)$ is the flexural rigidity per unit length of wall), these methods predict substantially lower dynamic pressures than those predicted for rigid walls (d_w=0) (Fig. 7a). Additionally, base flexibility (characterized by $d_\theta = GH^2/R_\theta$, where R_θ is the torsional spring constant) provides a modest decrease in dynamic pressure compared to walls rigidly constrained at the base (d_θ=0) (Fig. 7b). An elegant analysis by Younan and Veletsos [24] shows that the pressure distribution becomes roughly triangular with depth and the point of force application decreases from 0.6 H for a rigid wall to less than 0.3 H for a flexible cantilever wall (Fig. 7c). Increased foundation flexibility, i.e. increased rotational flexibility, has a similar effect (Veletsos and Younan [23]). These results provide theoretical support for the empirical observations of Mononobe and Matsuo [14] and they are consistent with the results of recent experimental studies described herein.

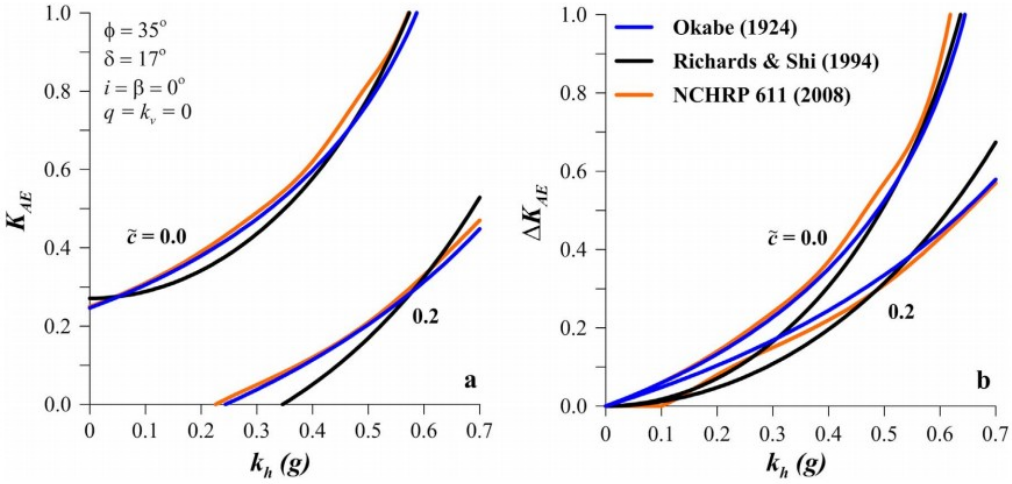

Fig. 5. Comparison methods: Okabe [3], Richards and Shi [17] and design recommendations in NCHRP 611 (Anderson et al. [18]). (a) Coefficient of total seismic load and (b) coefficient of dynamic earth pressure.

4. Experimental data

While the field observations following earthquakes are very valuable, one of the main limitations is that most commonly information on the actual design and construction is lacking. Hence, except in rare cases, e.g. Clough and Fragaszy [12], it is not possible to perform a rigorous back analysis of the observed performance. Therefore, experimental results are essential in order to be able to evaluate the validity of the various assumptions and the

applicability of the various methods of analysis. To this end the authors have been involved in an extensive program of centrifuge model experiments on different types of structures in both cohesionless and cohesive soils (Al Atik and Sitar [27], Sitar et al. [8], Mikola and Sitar [28], Candia and Sitar [29]). The centrifuge was chosen for the experimental program because it allows for consistent scaling of the critical parameters and the experiments are relatively economical in terms of time and cost. Most importantly, the scale of the models allows for the structures to be founded on soil (Fig. 8) and, consequently, avoid the rigid base foundation issue already discussed. Also, as seen in Fig. 8, the centrifuge provides an excellent environment for data collection and the models can be extensively instrumented with strain gauges, accelerometers, pressure sensors, etc. Overall, the experimental program involved a series of experiments with flexible and stiff U-shaped and cantilever structures retaining cohesionless and cohesive soils. All of these structures were 6.5 m high in prototype scale, representing typical height of walls used for highway structures. A separate set of experiments involved stiff, braced structures designed to mimic basement type walls in cohesionless soil. For brevity the specifics of scaling and experimental procedures are omitted herein, as they are described in detail in the publications referred to above. Instead the emphasis is on presentation of the results and their interpretation.

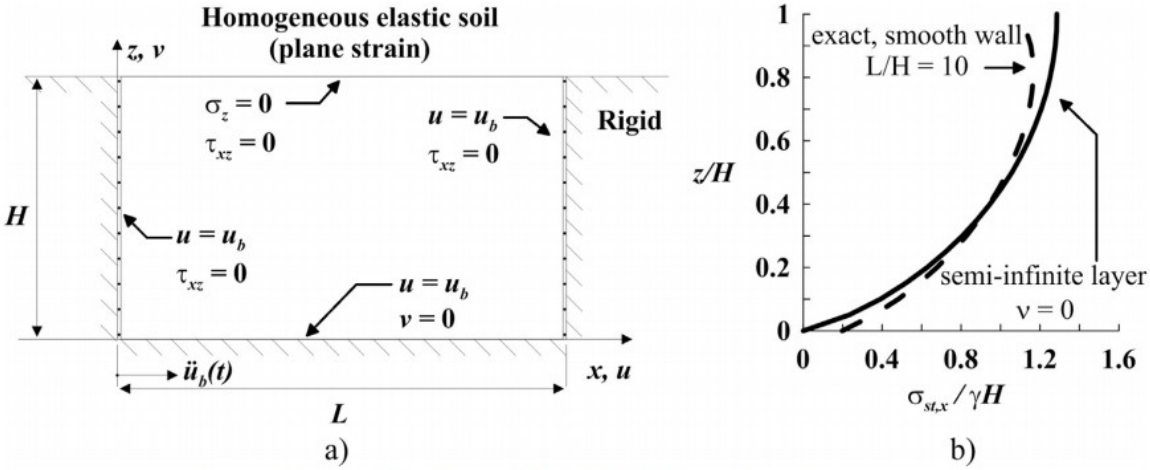

Fig. 6. a) Geometry of the problem solved by Wood [7]; b) Computed dynamic stress increment.

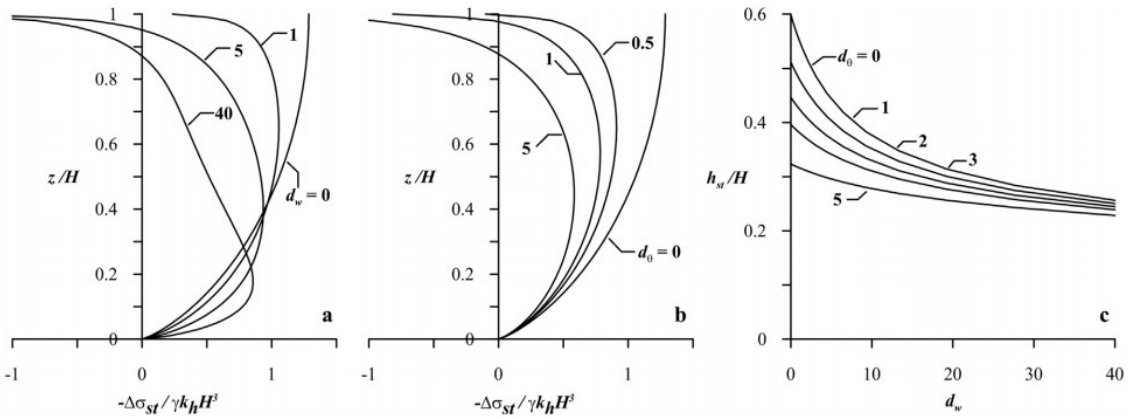

Fig. 7. a) Normalized wall pressure as a function of increasing wall flexibility (d_w); b) Normalized wall pressure as a function of increasing rotational flexibility (d_0) c) Location of the point of force application as a function of wall flexibility for cantilever walls. From Younan and Veletsos [23].

4.1. Dynamic earth pressures on stiff and flexible walls

The two types of structures shown in Fig. 8 are both cantilevers with the distinction that in the U-shaped channel configuration the wall is free to deflect but cannot translate or rotate about its base, whereas the free-standing cantilever wall can translate and rotate. While this distinction is important when it comes to the magnitude of the observed dynamic forces it did not seem to affect the distribution of the dynamic stress increment which was roughly triangular, increasing with depth, as illustrated in Fig. 9. The corresponding computed M-O and Seed and Whitman [5] (abbreviated as S & W) dynamic pressure increments are plotted for reference. This data shows that the point of application of the dynamic load increment on cantilever walls on a flexible foundation is roughly at 1/3 H as postulated by Mononobe and Matsuo [14] and computed analytically by Younan and Veletsos [24]. Similar observations were made in centrifuge experiments on cantilever walls by Ortiz et al. [30] and Stadler [31], and gravity walls by Nakamura [32]. Also, as can be seen, the point of application of the dynamic force at 0.6 H suggested by Seed and Whitman [5] procedure (S-W, “inverted triangle”) is not supported by the data.

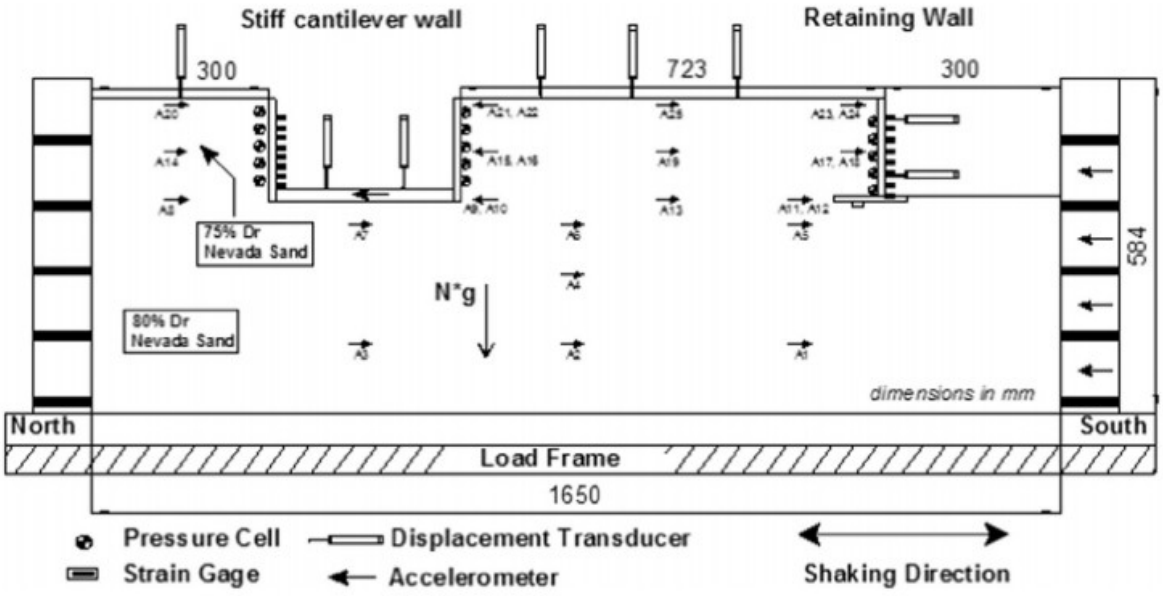

Fig. 8. Typical centrifuge model configuration, cohesionless backfill (Mikola and Sitar [28]).

A more direct way of evaluating the previously discussed conventional analysis procedures is to view the results in terms of the seismic earth pressure coefficient ΔK_{AE}. Fig. 10 is a summary of data obtained from centrifuge experiments with cohesionless soil by Mikola and Sitar [28] and compacted silty clay by Candia and Sitar [29]. The results are plotted against the peak acceleration in free field at the instant of maximum moment on the structure. The results show that the M-O solution and the S-W approximation provide a reasonable upper bound for stiff structures in cohesionless soil and are about 1/3 of what would have been obtained using the Wood [7] solution for rigid structures (Candia and Sitar [29]). Cohesion has a small, but measurable effect and, as the plot shows, the experiments with compacted silty clay backfill resulted in values at or below the mean of the data set. As would be expected, the observed seismic earth pressure coefficient for cantilever walls is significantly lower than what would be predicted by any of the conventional design methods, although there is no difference between cohesive and cohesionless backfill, which may be an artifact of the experimental procedure. Seed and Whitman [5] suggested that well designed gravity retaining structures should perform well at accelerations up to 0.3*g* without having been designed for seismic loading. The data for cantilever structures presented above supports their assertion, as the observed seismic earth pressure coefficient is very small for accelerations below 0.3*g*, as previously suggested by Al Atik and Sitar [27] and Sitar et al. [8].

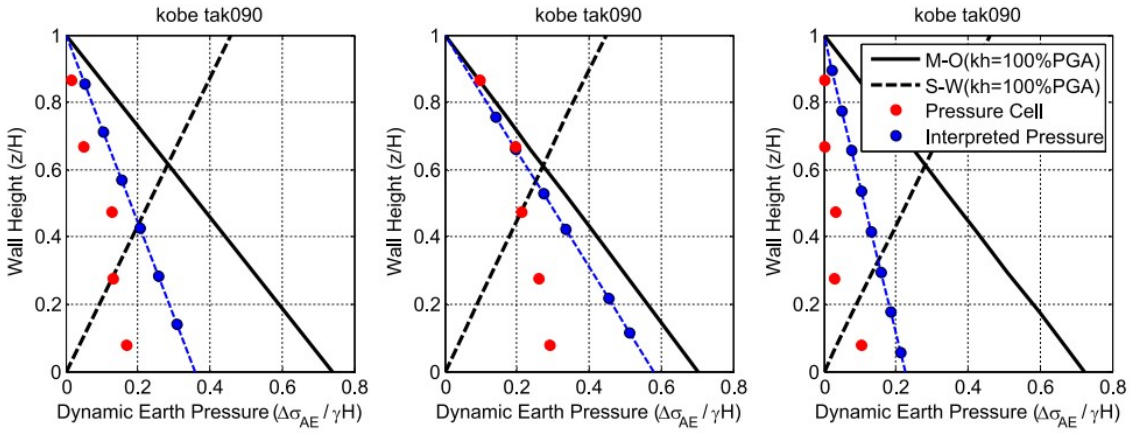

Fig. 9. Dynamic earth pressure distributions directly measured and interpreted from the pressure sensors and strain gage and load cell data and estimated M-O and S & W values (PGA_{ff} =0.61 gMikola and Sitar [28]).

4.2. Dynamic earth pressures on deep stiff walls

The results discussed above are applicable to relatively shallow structures up to about 7 m in height/depth and it may be reasonable to extrapolate these results to taller free-standing retaining structures in level ground. However, the same is not possible for more deeply embedded walls, such as deep basement walls, since the seismic earth pressure increment is bound to decrease with depth. To evaluate this particular problem a set of centrifuge experiments was performed on a very stiff braced deep wall, 13.3 m deep and founded on 5.5 m of medium dense sand in prototype dimensions. The structure consisted of two thick walls with three levels of stiff cross braces, as shown in Fig. 11. The bracing was instrumented with load cells in order to obtain a direct measurement of loads because the readily available earth pressure sensors, while providing satisfactory relative values, do not provide reliable absolute values. Consequently, the structure was very stiff, albeit not completely rigid. Other instrumentation included accelerometers and LVDT's to measure site response and to measure transient and permanent deformations and all tests were performed at 36*g*. In contrast to the experiment layout for the shallow embedded structures (Fig. 8), the structure was placed in the center of the container in order to minimize any potential boundary effects due to the additional height of the structure.

Fig. 12 shows the dynamic lateral earth pressures observed in two shaking events in the centrifuge. The dynamic load measured in the top row of load cells was assumed to correspond to dynamic pressure starting at zero at the surface and increasing linearly with depth until the depth at the midpoint between the top and middle row of load cells. The dynamic load measured in the middle and bottom rows of load cells was then combined and distributed linearly from the midpoint between the top and middle row of load cells to the base of the wall. As can be seen, the dynamic earth pressure distribution at the instant of maximum dynamic earth pressure resultant is approximately equal to K_o in the upper part of the deposit, reaching a maximum of about 0.15 γH to 0.2 γH at about 0.3 H. It then decreases with

depth to essentially zero at the base of the wall. The dynamic earth pressure distribution at the instant of minimum dynamic earth pressure resultant is also shown. The principal difference between the two events is the number of cycles during which the distribution approaches the maximum is much greater for the Kobe-Takatori record than for Loma Prieta record, while the distributions at the instant of maximum dynamic earth pressure increment are similar. In addition, dynamic pressure distributions computed using the M-O and S & W methods are included for comparison. The peak depth-averaged acceleration is used as the seismic coefficient in the M-O computation and 80% of the PGA at the surface is used as the seismic coefficient in the S & W computation.

The depth-averaged acceleration better accounts for the incoherency and wave scattering as the depth of embedment increases. In fact, Anderson et al. [18] developed a depth dependent modification of the seismic coefficient for use in the M-O method for retaining walls, summarized in Eq. (5)

$$k_{avg}=\alpha k_{max}\alpha=1+0.01H[(0.5\beta)-1] \quad (5)$$

$$\rho_i=\rho_{min}+(\rho_{max}-\rho_{min})\left(\frac{z_i}{H}\right)^{1/2}(\mathbf{a}) \qquad n_i=n_{min}+\Delta n\left(\frac{\sigma_{m,i}}{P_a}\right)^{1/2}(\mathbf{b})dfac_i$$

$$=dfac_{min}+\Delta dfac\left(\frac{\sigma_{m,i}}{P_a}\right)^{1/2}(\mathbf{c}) \qquad e_i=\frac{G_s}{\rho_i}-1(\mathbf{d})G_{r,i}$$

$$=\frac{625}{0.3+0.7e_i^2}P_a(\mathbf{e}) \qquad G_{max,i}=G_{r,i}\left(\frac{\sigma_{m,i}}{P_a}\right)^{1/2}(\mathbf{f}) \quad (6)$$

where k_{max} is the peak seismic coefficient measured at the ground surface ($=F_aPGA$), α is the fill height-dependent reduction factor, H is the backfill height in feet (applicable up to height 100 ft=30 m), $\beta = F_vS_1/k_{max}$, F_a is the short (0–2 s) period range site coefficient ($=f(S_s$, site class)) from FEMA 750 [2], F_v is the 1-second period site coefficient ($=f$ (S_1, site class)) from FEMA 750 [2], S_s is the mapped short period spectral acceleration, and S_1 is the 1-second period spectral acceleration. Values of β equal to 0.5, 1.0, and 1.5 correspond roughly to lower, median, and upper bound estimates of design site response spectra with increasing long period input. Fig. 13 shows the reduction factor α computed using experimental data from Mikola and Sitar [28] (denoted by RG01), Candia and Sitar [29] (denoted by GC01) and for the current study (denoted by NW01) for the braced basement structures compared to the bounds presented in Anderson et al. [18]. There is good agreement between the observed and predicted values.

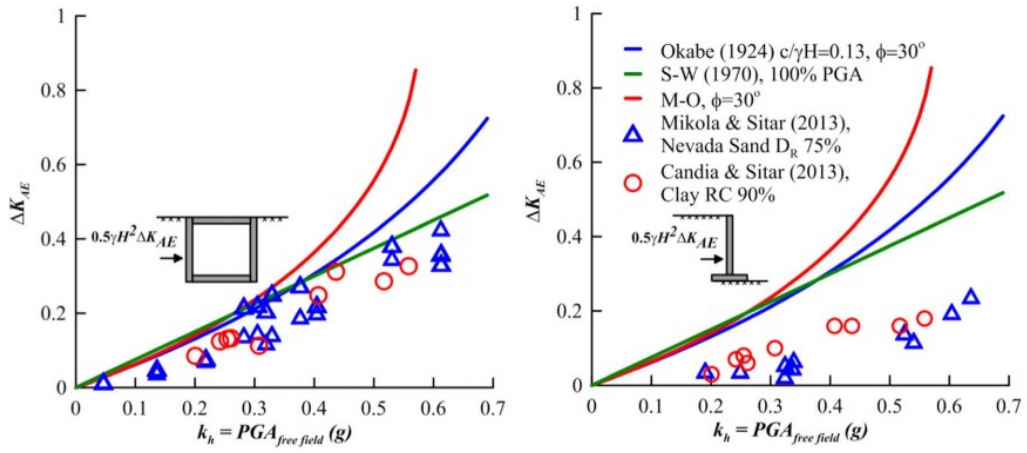

Fig. 10. Seismic earth pressure coefficients from centrifuge model tests for stiff walls in cohesionless and cohesive soil (left) and corresponding results for cantilever walls (right)..

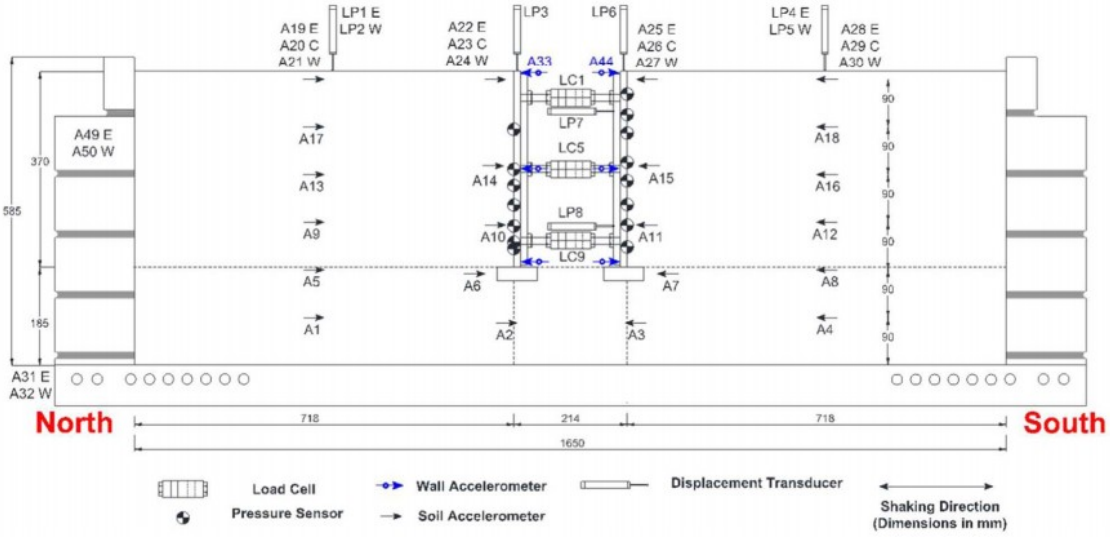

Fig. 11. Layout of the centrifuge model of a deep stiff structure..

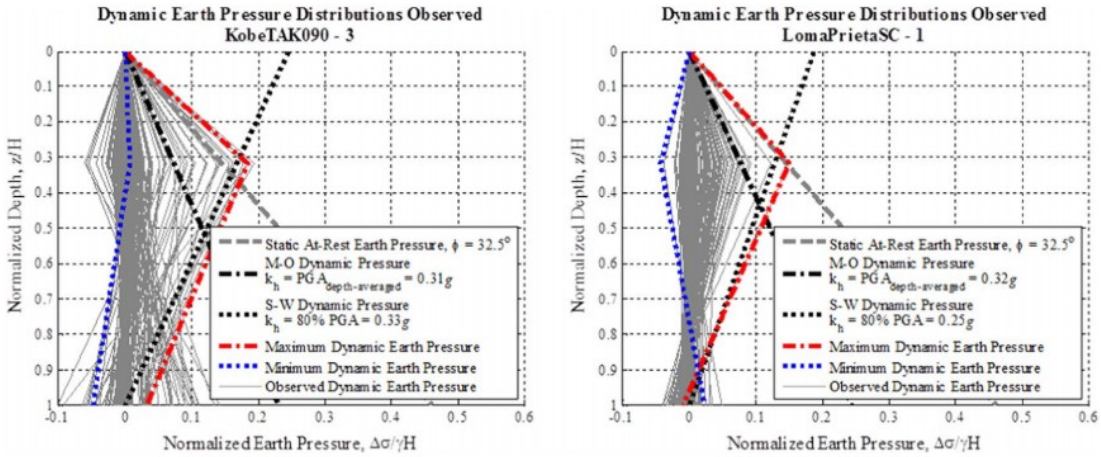

Fig. 12. Dynamic earth pressure increment distribution for two different events as a function of depth from centrifuge experiments on a deeply embedded structure.

Using the peak depth-averaged acceleration (k_{MHEA}) as the seismic coefficient, the seismic earth pressure coefficient computed from the experimental data matches well with the M-O predictions. An added benefit of using depth-averaged acceleration is that the height of the wall is implicitly accounted for, as the response of deeper parts of the backfill is incorporated into the computation. Additionally, depth-averaged acceleration is more appropriate when comparing experimental data to limit-state methods in that the sliding wedge is assumed to be rigid, so a representative acceleration measured over the volume of the wedge is necessary. This effect becomes more pronounced as the height of the wall becomes larger. Fig. 14 shows the seismic earth pressure coefficients from previous experimental studies by Mikola and Sitar [28] and Candia and Sitar [29], Fig. 10, as well as the current study using the peak depth-averaged acceleration as the ordinates.

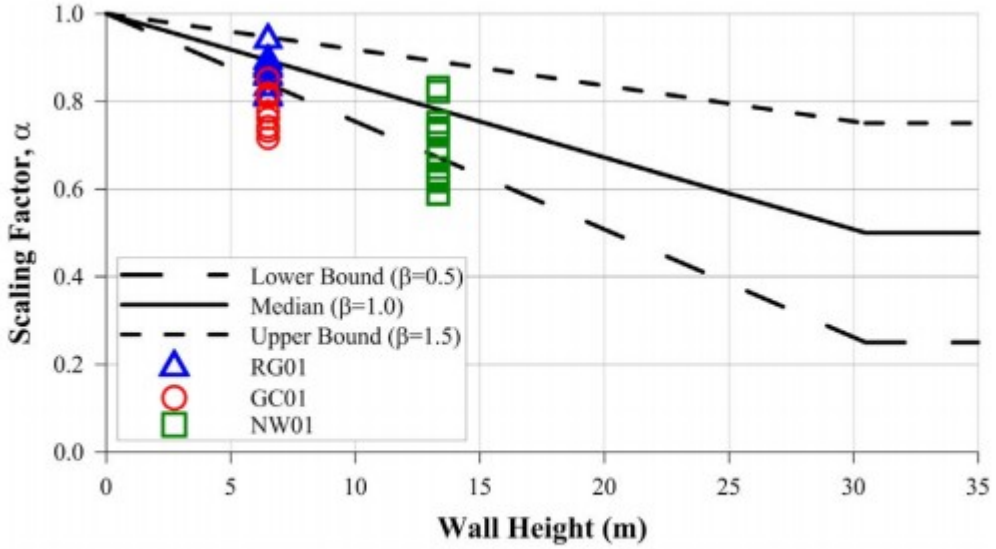

Fig. 13. Code-based (Anderson et al. [18]) and observed height-dependent seismic coefficient reduction factor versus wall height.

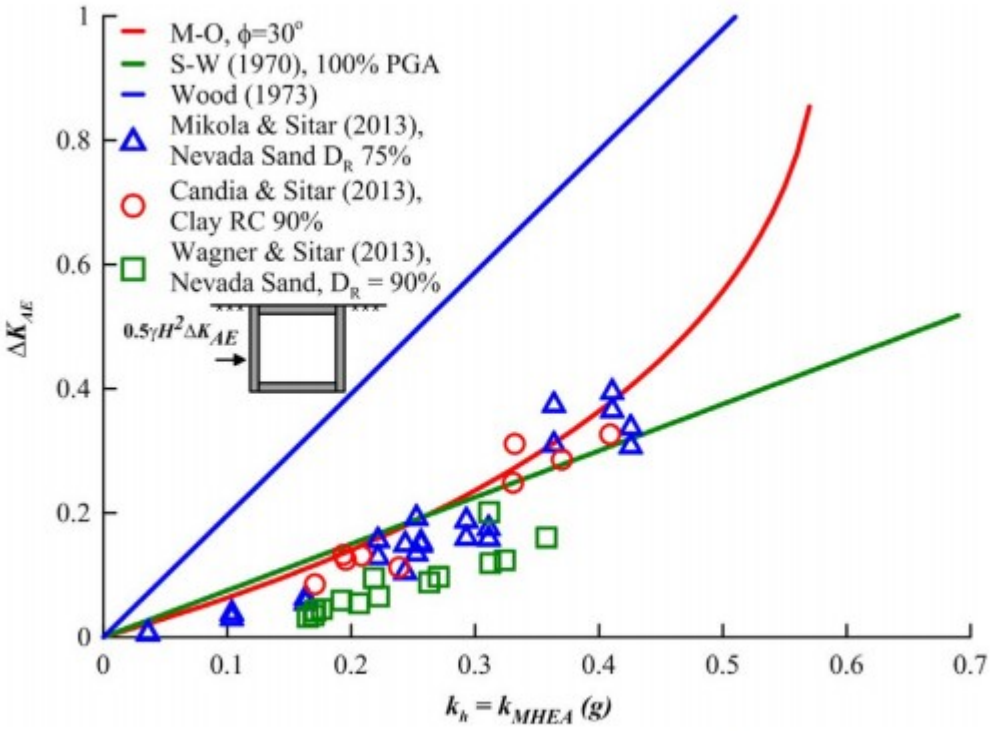

Fig. 14. Seismic earth pressure coefficients from centrifuge model tests for stiff walls in cohesionless and cohesive soil versus peak depth-averaged acceleration (k_{MHEA}).

5. Numerical simulation

A numerical model was developed in FLAC$^{2\text{-}D}$ [33] to simulate the centrifuge experiment of the deep stiff structure. The nonlinear, hysteretic soil model UBCHyst (see Naesgaard [34]) was used to simulate the dynamic response of the soil, and was initially calibrated to match Darendeli [35] shear modulus degradation curves, and then adjusted further to match the acceleration response in the free field of the centrifuge experiment. The maximum shear modulus and the bulk modulus were reduced by half in the two columns of soil zones immediately adjacent to the sides of the structure to account for permanent softening in the centrifuge experiment. This was necessary to calibrate the acceleration response in the soil and structure based on the results from the centrifuge experiment. A fortuitous consequence was that better agreement between the magnitude of the dynamic earth pressure resultant measured in the centrifuge experiment and computed in the numerical model was observed. The structure was modeled using linear elastic beam elements and was rigidly attached to the soil grid because gapping was not observed between the backfill and the structure. Interface elements were used initially as in previous numerical simulations (Mikola and Sitar [28], Candia and Sitar [29]) to allow for sliding; however, the greater depth of the structure required increasing interface normal stiffness with depth, which is not currently feasible in FLAC$^{2\text{-}D}$ [33]. The mesh is shown in

Fig. 15 and the structural and soil properties are shown in Table 1 and Table 2 respectively. The boundary conditions were selected to match the centrifuge experiment; i.e., the base was rigid and the sides of the domain were attached together. Rayleigh damping was specified as ξ_{min}= 2.0% in the soil grid and ξ_{min} = 0.01% in the structural elements at a center frequency of 3.0 Hz to match the initial estimated site period in the free field. It was determined in the calibration process that varying the soil parameters with depth provided a more accurate simulation of the acceleration response; the variation with depth utilized in this study is shown in Eq. (6)a-e, where the i^{th} layer is denoted by a subscript. The focus of the calibration process was to select reasonable soil properties and distributions that could be obtained from accepted correlations; e.g., the Hardin [36] relation between reference shear modulus and void ratio, and properties increasing with the square root of the depth (z_i) or mean confining pressure ($\sigma_{m,i} = (\sigma_{x,i} + \sigma_{y,i} + \sigma_{z,i})/3$).

Table 1
Structural element properties used in FLAC model of centrifuge test.

Property per unit width	Units	Basement Wall	Cross Braces	Footing
Elastic Modulus	E* (kPa)	7.68×10^{7}	7.68×10^{7}	7.68×10^{7}
Unit mass	ρ (Mg/m^3)	2.84×10^{0}	3.34×10^{1}	2.72×10^{0}
Cross Sectional Area	A (m^2/m)	5.75×10^{-1}	9.53×10^{-3}	9.14×10^{-1}
Second Moment of Area	I (m^4/m)	2.97×10^{-2}	9.17×10^{-4}	6.43×10^{-2}

* E=E/(1-v2) equivalent plane strain elastic modulus for aluminum.

The seismic earth pressure coefficient was calculated using two methods. In the first method, the axial load in the struts was summed and the dynamic component was evaluated; this is the same procedure used in the centrifuge experiments on braced structures. In the second method, the horizontal stresses in the soil zones adjacent to the structure were recorded and integrated over the height of the structure. The dynamic earth pressure distribution computed in the numerical simulation by distributing the strut loads is compared with the dynamic earth pressure distribution measured in the centrifuge experiment in Fig. 16. The seismic coefficients (k_h) and seismic earth pressure coefficients (ΔK_{AE}) computed in the numerical model were then compared to the experimental data in Fig. 17. As can be seen, the results of the numerical simulations agree well with the experimental data.

6. Conclusions

A review of traditional methods of analysis shows that the flexibility of the retaining structure and that of its foundation plays a very important role in the magnitude of the predicted seismic loads and that their magnitude significantly decreases with increased wall flexibility. This has been first noted by Mononobe and Matsuo [14] and since then shown to be the case

analytically by Younan and Veletsos [24] among others. The results of an extensive set of centrifuge experiments modeling retaining structures with cohesionless and cohesive backfill and observations of seismic performance of conventional retaining structures provide further support for these conclusions. Moreover the line of action of the resulting forces is shown to be roughly at 1/3 H for typical cantilever or gravity retaining structures of moderate height.

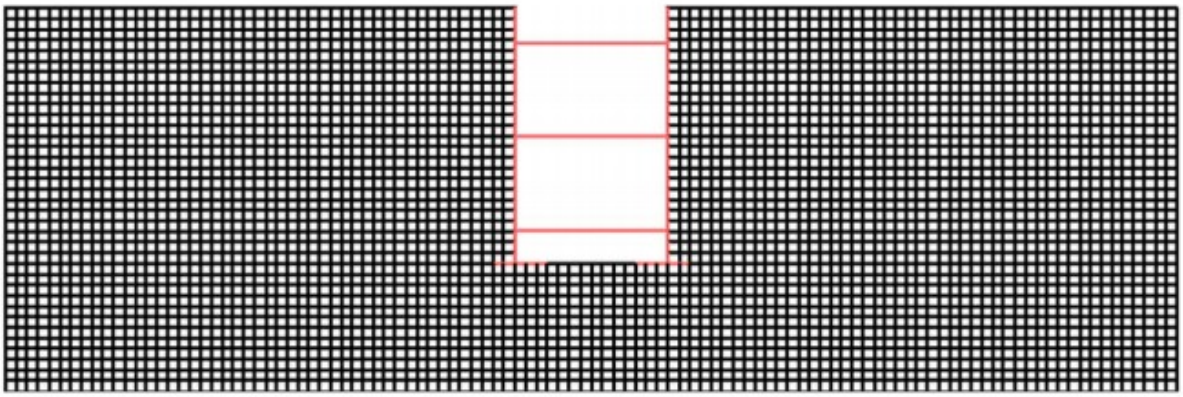

Fig. 15. Two-dimensional finite difference mesh of centrifuge test developed in FLAC.

Table 2
Calibrated soil model properties used in FLAC model.

ρ_{min}	=	1.66	Mg/m^3	P_a	=	100	kPa	K_i	=	$2G_{max,i}$	rm	=	0.75
ρ_{max}	=	1.7125	Mg/m^3	ψ	=	0.0	deg	R_f	=	0.75	$n1$	=	1.25
c	=	0.0	kPa	n_{min}	=	1.75		$dfac_{min}$	=	0.00	G_s	=	2.66
ϕ_f	=	32.5	deg	Δn	=	1.884		$\Delta dfac$	=	0.5657	mod 1	=	0.75

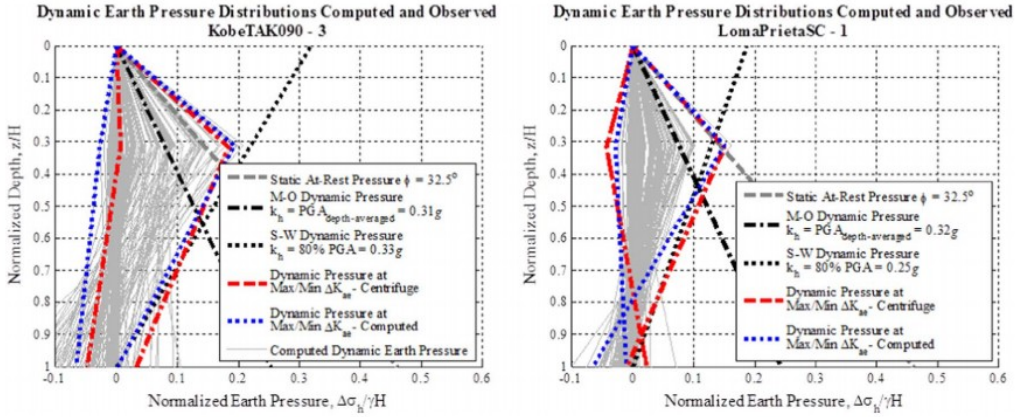

Fig. 16. Dynamic earth pressure distribution computed in numerical simulation compared to that measured in centrifuge experiment for two different events on a deeply embedded structure..

The results of recently completed centrifuge experiments on a model of a deeply embedded, stiff, retaining structure show that seismic earth pressures increase only moderately with depth to a depth of about 0.3 H and then decrease to a small fraction of the static pressure at depth. This observation is supported by the result of numerical (FLAC$^{2\text{-}D}$) simulations of

the centrifuge experiments. The experimental results also show that the traditionally used MononobeOkabe and Seed and Whitman [5] methods of analysis provide a reasonable upper bound for predicted seismic loads on retaining structures In addition, depth-averaged acceleration appears to be an appropriate measure in determining the equivalent seismic earth pressure coefficient with the Mononobe-Okabe and Seed and Whitman [5] methods and it is consistent with the original assumptions of those methods. In contrast, there is no evidence to support the further use of the Wood [7] solution and its derivatives except in special cases of very stiff structures on very stiff or rock foundation with relatively loose backfill.

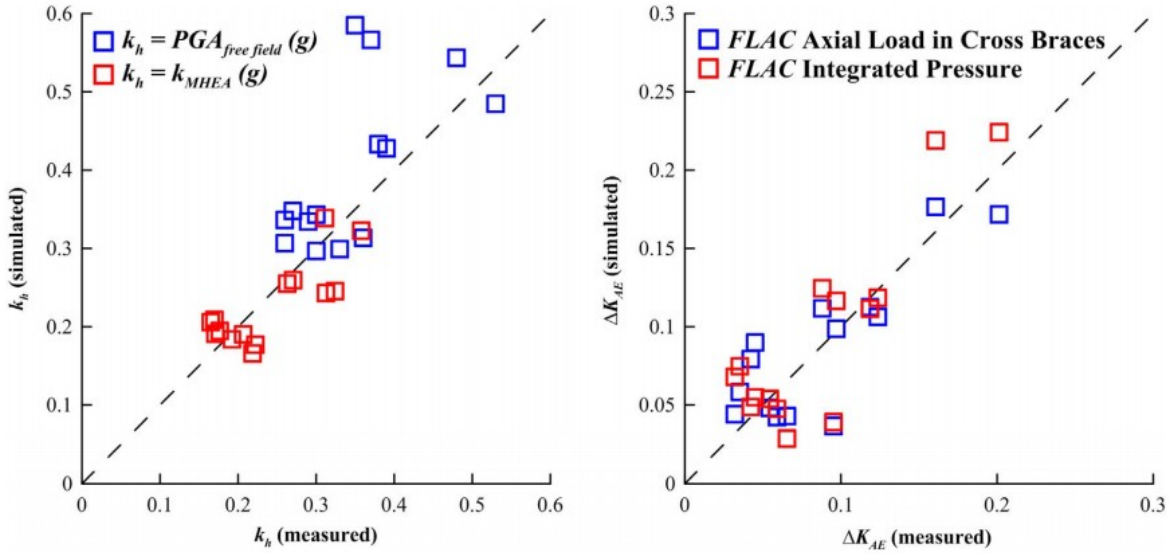

Fig. 17. Seismic coefficients (k_h) and seismic earth pressure coefficients (ΔK_{AE}) from numerical model and centrifuge model tests on basement walls.

Finally, due to the complexity of the various types of retaining structures, ultimately, well instrumented and documented case histories are needed to fully assess the range of potential problems and their solutions.

Acknowledgments

The funding for this research was provided in part by a grant from the California Geotechnical Engineering Association (CalGeo), the State of California Department of Transportation (Caltrans) Contract No. 65N2170, NSF-NEES-CR Grant No. CMMI-0936376: Seismic Earth Pressures on Retaining Structures, and the Edward G. Cahill and John R. Cahill Endowed Chair Fund. The authors also thank two anonymous reviewers for their thoughtful and constructive comments.

References

[1] International Code Council (ICC) . International existing building code. Illinois: Country Club Hills; 2011.

[2] Building Seismic Safety Council . NEHRP recommended seismic provisions for new buildings and other structures (FEMA P-750), 2009 edition. Washington, DC: BSSC; 2009.

[3] Okabe S. General theory of earth pressure. J Jpn Soc Civ Eng 1924;6:1277–323.

[4] Mononobe N, Matsuo M. “On the Determination of Earth Pressures during Earthquakes,”. Proc World Eng Congr 1929;9:179–87.

[5] Seed HBWhitman RV. “Design of Earth Retaining Structures for Dynamic Loads,” ASCE Specialty Conference, Lateral Stresses in the Ground and Design of Earth Retaining Structures, Cornell Univ., Ithaca, New York, 103–147; 1970.

[6] Mylonakis G, Kloukinas P, Papatonopoulos C. An alternative to the MononobeOkabe equation for seismic earth pressures. Soil Dyn Earthq Eng 2007;10(27):957–69.

[7] Wood JH. Earthquake induced soil pressures on structures [Phd thesis]. Pasadena, CA: California Institute of Technology; 1973.

[8] Sitar NMikola RGCandia G. “Seismically Induced Lateral Earth Pressures on Retaining Structures and Basement Walls”, Geotechnical Engineering State of the Art and Practice, Keynote Lectures from GeoCongress 2012, GSP 226, ASCE; 2012.

[9] Lew MSitar NAl Atik L. Seismic Earth Pressures: Fact or Fiction. Invited Keynote Paper, Earth Retention Conference, ER 2010, ASCE, Seattle; 2010.

[10] Kendal Riches L. Observed Earthquake Damage to Christchurch Cit Council Owned Retaining Walls and the Repair Solutions Developed Proceedings of the 6th International Conference on Earthquake Geotechnical Engineering (6ICEGE), Christchurch, NZ, November 1-4, 10 ; 2015.

[11] Verdugo R, Sitar N, Frost JD, Bray JD, Candia G, Eldridge T, Hashash Y, Olson SM, Urzua A. Seismic performance of earth structures: dams, levees, tailings dams and retaining walls. Earthq Spectra 2012(28):S75–S96.

[12] Clough GWFragaszy RF. “A Study of Earth Loadings on Floodway Retaining Structures in the 1971 San Fernando Valley Earthquake,” Proceedings of the Sixth World Conference on Earthquake Engineering, Vol. 3; 1977.

[13] Kramer SL. Geotechnical earthquake engineering. New Jersey: Prentice Hall; 1996.

[14] Mononobe N, Matsuo M. Experimental investigation of lateral earth pressures during earthquakes, Vol. X. Tokyo: Bull. Earthq. Res. Ins; 1932. p. 884–902.

[15] Sherif MA, Ishibashi I, Lee CD. Earth pressure against stiff retaining walls. J Geotech Eng 1982;108:679–95.

[16] Chen WF, Liu XL. Limit analysis in soil mechanics. Elsevier; 1990.

[17] Richards R, Shi X. Seismic lateral pressures in soils with cohesion. J Geotech Eng 1994;7:1230–51.

[18] Anderson DG, Martin GR, Lam IP, Wang JN. Seismic design and analysis of retaining walls, buried structures, slopes and embankments [NCHRP Report 611]. Washington, D.C: Transportation Research Board, NCHRP; 2008.

[19] Matsuo HOhara S. Lateral Earth Pressure and Stability of Quay Walls During Earthquakes, Proceedings, Second World Conference on Earthquake Engineering, Vol. 1, Tokyo, Japan; 1960.

[20] Prakash S. “Dynamic Earth Pressures,” State of the Art Report - International Conference on Recent Advances on Geotechnical Earthquake Engineering and Soil Dynamics, St. Louis, Missouri, Vol. III, 993-1020; 1981.

[21] Ostadan F, White WH. Lateral Seismic Soil Pressure-An Updated Approach. In Preproceedings of UJNR Workshop on Soil-Structures Interaction, U.S. Geological Survey, Menlo Park, California; 1998.

[22] Ostadan F. Seismic soil pressure for building walls – an updated approach. J Soil Dyn Earthq Eng 2005(25):785–93.

[23] Veletsos AS, Younan AH. Dynamic response of cantilever retaining walls. J Geotech Geoenviron Eng 1997;2(123):161–72.

[24] Younan AH, Veletsos AS. Dynamic response of flexible retaining walls. Earth Eng Struct Dyn 2000;29:1815–44.

[25] Zeng X. Modelling the behavior of quay walls in earthquakes [PhD. thesis]. Cambridge, England: Cambridge University; 1990.

[26] Steedman RSZeng X. “The Seismic Response of Waterfront Retaining Walls,” Design and Performance of Earth Retaining Structures, Conference Proceedings, Cornell University, Ithaca, New York, June 18-21, ASCE Geotechnical Special Publication No. 25; 1990.

[27] Al Atik L, Sitar N. Seismic earth pressures on cantilever retaining structures. J Geotech Geoenviron Eng 2010;136(10):1324–33.

[28] Mikola RGSitar N. Seismic Earth Pressures on Retaining Structures in Cohesionless Soils. Report No. UCB GT 13-01, UC Berkeley, March 2013, http://dx.doi.org/ 10.13140/RG.2.1.1524.1446.

[29] Candia GSitar N. Seismic Earth Pressures on Retaining Structures in Cohesive Soils. Report No. UCB GT 13-02, August 2013, 161p;UC Berkeley, August 2013, http://dx.doi.org/10.21418/G8159F.

[30] Ortiz LA, Scott RF, Lee J. Dynamic centrifuge testing of a cantilever retaining wall. Earthq Eng Struct Dyn 1983;11:251–68.

[31] Stadler AT. Dynamic centrifuge testing of cantilever retaining walls [PhD thesis]. Boulder, CO: University of Colorado at Boulder; 1996.

[32] Nakamura S. Reexamination of Mononobe-Okabe Theory of gravity retaining walls using centrifuge model tests. Soils Found 2006;2(46):135–46.

[33] Itasca Consulting Group, Inc . Fast Lagrangian analysis of continua, version 7.0. [computer software]. Minneapolis, Minnesota: Itasca Consulting Group, Inc; 2011.

[34] Naesgaard E. A hybrid effective stress – total stress procedure for analyzing soil embankments subjected to potential liquefaction and flow [Ph.D. thesis]. Vancouver, Canada: University of British Columbia; 2011.

[35] Darendeli M. Development of a new family of normalized moduli reduction and material damping curves [Ph.D thesis]. Austin, TX: University of Texas at Austin; 2001.

[36] Hardin BO. The nature of stress-strain behavior of soils. Proceedings of Earthquake Engineering and Soil Dynamics, ASCE, Pasadena, California, Vol. 1, pp. 3-89; 1978.